Revealing Defect-State Photoluminescence in Monolayer WS_2 by Cryogenic Laser Processing

*Zhengyu He[1], Xiaochen Wang[1], Wenshuo Xu[1], Yingqiu Zhou[1], Yuewen Sheng[1], Youmin Rong[1], Jason M. Smith[1], Jamie H. Warner[1]**

[1]Department of Materials, University of Oxford, Parks Road, Oxford, OX1 3PH, United Kingdom

*Jamie.warner@materials.ox.ac.uk;

Abstract.

Understanding the stability of monolayer transition metal dichalcogenides in atmospheric conditions has important consequences for their handling, life-span and utilization in applications. We show that cryogenic photoluminescence spectroscopy (PL) is a highly sensitive technique to the detection of oxidation induced degradation of monolayer tungsten disulfide (WS_2) caused by exposure to ambient conditions. Whilst long term exposure to atmospheric conditions causes massive degradation from oxidation that is optically visible, short term exposure produces no obvious changes to the PL or Raman spectra measured at either room temperature or even cryogenic environment. Laser processing was employed to remove the surface adsorbents, which enables the defects states to be detected *via* cryogenic PL spectroscopy. Thermal cycling to room temperature and back down to 77 K shows the process is reversible. We also monitor the degradation process of WS_2 using this method, which shows that the defect related peak can be observed after one month ageing in ambient conditions.

KEYWORDS Tungsten Disulfide, photoluminescence, defects, 2D semiconductors

Monolayer transition metal dichalcogenides (TMDs) have attracted great interest due to it exotic physical properties including large spin-orbit coupling, strong quantum confinement and the indirect-

to-direct bandgap crossover for monolayer.[1,2] This leads to valley polarization,[3–5] unexceptionally large excitonic effect,[6,7] and bright photoluminescence (PL) even at room temperature.[8,9] These properties make monolayer TMDs an attractive building block to fabricate atomically thin electronics and optoelectronics, such as valleytronics,[10] photodetector,[11–13] solar cell,[14–17] and light-emitting diode (LED).[14,16,18,19]

A critical aspect of the effective implementation of monolayer TMDs in applications is their stability and processing capability. Air sensitive samples pose significantly greater challenges in large scale fabrication and handling. The modification of TMDs properties by exposure to ambient atmospheric conditions is important for the time-dependent variable performance of devices. This argument especially applies to 2D materials which possesses ultrahigh surface area to volume ratios. For instance, Kim *et al.*[20] reported that freshly prepared multilayer graphene oxides were metastable, with a 1-month relaxation process with structure and chemistry evolution. Few-layer black phosphorus (BP) is another example of a layered materials which suffers greatly from degradation in ambient conditions. Wood *et al.*[21] and Doganov *et al.*[22] observed that the mobility ratio between freshly prepared and aged few-layer BP could be up to 10^4. Aging in ambient condition can also impact the performance of topological insulator or even graphene which was once believed to be chemically inert.[23-25]

Recent work on monolayer TMDs has shown that exposure to UV light in a humid environment causes degradation through oxidation.[26] Grain boundaries are the first to be degraded due to the presence of non-hexagonal ring structures that are less stable. Rong *et al.*[27] showed that monolayer WS_2 can be heated in air to reveal its grain boundaries between merged domains grown by chemical vapour deposition. Both of these studies indicate that monolayer TMDs could have some instability when left

out in air (oxygen rich) and in natural light (containing UV). Therefore developing methods that can detect changes in monolayer TMDs from exposure to ambient conditions is important.

In this paper, we examine the onset of degradation within monolayer WS_2 under ambient condition, which occur on a much longer time scale compared with black phosphorus.[21,22] Starting at the nanoscale, degradation expands gradually with increasing aging time and eventually becomes optically visible, leading to reduced PL. However, before the degradation area becomes optically visible, these defects cannot be easily detected by simple morphological or spectroscopic methods, such as SEM, AFM or room temperature PL or Raman spectroscopy. Here we use cryogenic PL spectroscopy to probe PL from defect states in WS_2 domains. A laser induced cleaning process is employed to remove the surface adsorbents and a new peak emerges that is associated with defects in monolayer WS_2.

Results and discussion

Monolayer WS_2 single crystals were grown on silicon wafer with 300 nm oxide layer using previously reported method.[28] They were left in air under natural room light conditions to age. Figure 1(a)-(c) shows the optical images of typical domains of as-grown, 2-month aged and 8-month aged in ambient condition monolayer tungsten disulfide (WS_2) crystals. As-grown and 2-month aged crystals have very uniform optical contrast. However, the 8-month aged WS_2 has lots of granular structures not seen in the other two samples. Figure 1(d)-(f) showed the SEM images of monolayer WS_2 with different aging time. Similar to optical image, as-grown monolayer WS_2 has uniform contrast in the SEM (figure 1(d)). 2-month aged crystal also has high uniformity, with only a few small particles on top and some rough edges, shown in figure 1(e). Figure 1(f) shows that grains possessing lighter contrast in the 8-month aged monolayer WS_2 domain with decreasing density from crystal edges to the central area. To further investigate the surface morphology quantitatively, we performed atomic force microscopy (AFM) characterization on these three types of monolayer WS_2 and typical examples were presented in figure 1(g)-(i). In figure 1(g),(h), both as-grown and 2-month aged crystals showed uniform surface

morphology despite small particles on the 2-month aged sample which is believed to come from unintentional contaminant during storage in ambient conditions. However, in figure 1(f), variations in height between regions with lighter and normal WS_2 optical and SEM contrast was observed on 8-month aged crystal. The height profile across one of the light-contrast grains labeled by blue dashed line in the inset of figure 1(f), shows that it was 3.5 nm higher than surrounding monolayer WS_2 sheet. Typical values ranged from 1.5 nm to 4.5 nm. It should be made clear that these results are taken from different typical crystals instead of the same domain.

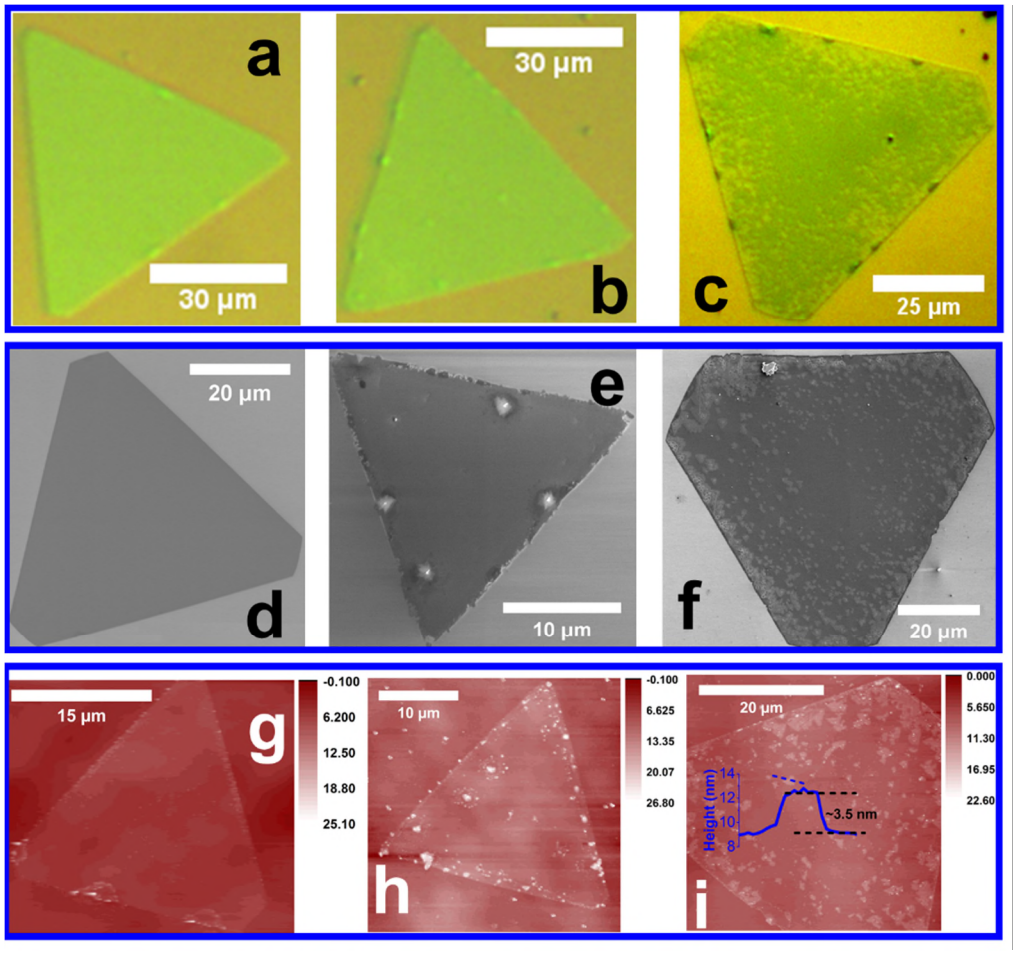

Figure 1. (a-c) Optical images of (a) as-grown, (b) 2-month aged and (c) 8-month aged monolayer WS_2. (d-f) SEM images of (d) as-grown, (e) 2-month aged and (f) 8-month aged monolayer WS_2. (g-i) AFM surface morphology images of (g) as-grown, (h) 2-month aged and (i) 8-month aged monolayer WS_2. The Inset in (i): Height profile of area with light optical contrast across the blue dash line. The height of the grain was about 3.5 nm.

In figure 2, we presented integrated intensity map of both PL and two characteristic Raman vibration modes, A_{1g} and E^1_{2g} of as-grown, 2-month and 8-month aged monolayer domains at room temperature. The PL and Raman intensities of both as-grown and 2-month aged crystal have high uniformity while noticeable intensity variations can be observed in 8-month aged sample. Carefully comparing the intensity map with optical image revealed that area with weaker PL or Raman response in figure 2(j)-(l) corresponded to areas with lighter optical contrast in figure 2(i). This indicates that aging in air can lead to degradation within monolayer WS_2 where it can either be oxidized,[29,30] or etched away by water vapor,[31] followed by contamination adsorption. Such a process starts preferentially from the edges, likely due to the increased dangling bonds and therefore enhanced catalytic efficiency of WS_2 edge states.

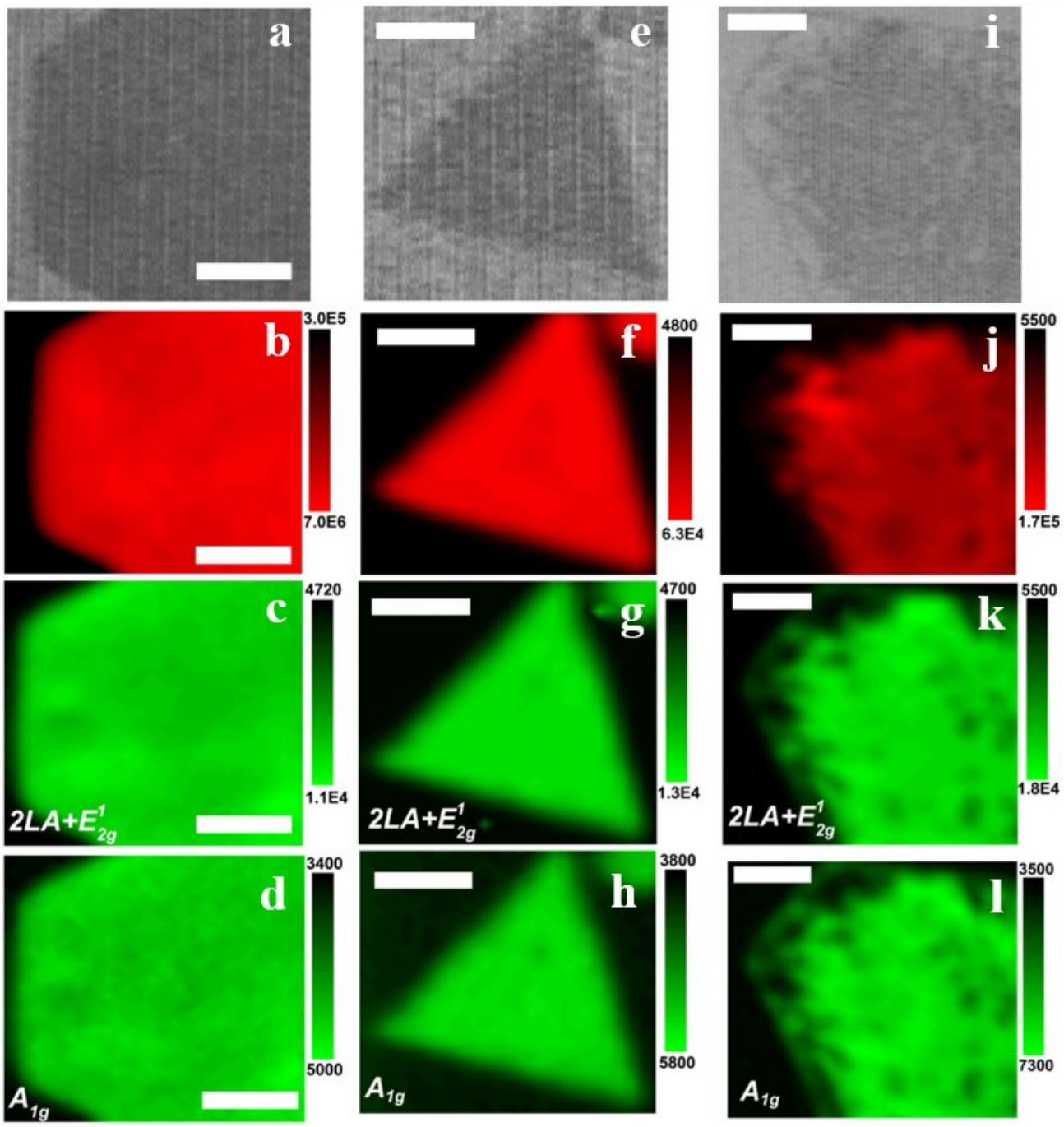

Figure 2. 2D spatial mapping of PL and Raman signals for monolayer WS_2 with different aging time at room temperature. (a-d) Maps for as-grown WS_2 sample. (a) Optical image, (b) PL integrated intensity map, (c) $2LA+E_{2g}^1$ intensity map, and (d) A_{1g} map of as-grown sample. Scale bar: 10 um. (e-h) Spectroscopic map of 2-month aged sample. (e) Optical image, (f) PL integrated intensity map, (g) $2LA+E_{2g}^1$ Raman intensity map, and (h) A_{1g} Raman intensity map. Scale bar: 15 um. (i-l) Optical image and spectroscopic map of 8-month aged

sample. (i) Optical image, (j) PL integrated intensity map, (k) 2LA+E_{2g}^1 Raman intensity map, and (l) A_{1g} Raman intensity map. Scale bar: 10 μm.

The observation of degradation motivates the development of characterization methods that are highly sensitive to the onset of the defects in monolayer WS_2. Raman spectroscopy is an powerful tool to characterize the defects in graphene with addition D peak arising in defective regions.[32] In figure 3(a),(b), we presented normalized Raman spectra from area with similar optical contrast of both freshly made and 8-month aged sample at room temperature. No obvious difference can be observed for the overall spectra. We deconvolved the Raman spectra to extract the contributions of different vibration modes, but hardly any difference were distinguished.[33] The origins of the peaks in the Raman spectrum is presented in supporting information. Defects have been reported to alter the luminescent properties of TMDs.[31,34,35] Figure 3(c),(d) showed the PL spectra of fresh and aged monolayer WS_2 at room temperature. The PL emission of aged sample is weaker and slightly blue-shifted under similar excitation conditions. However, it cannot serve as an indicator of the existence of defects since such

an intensity and peak position variation have been observed in the different regions on one as-grown monolayer crystal.[8] Apart from that, no noticeable PL shape change can be distinguished.

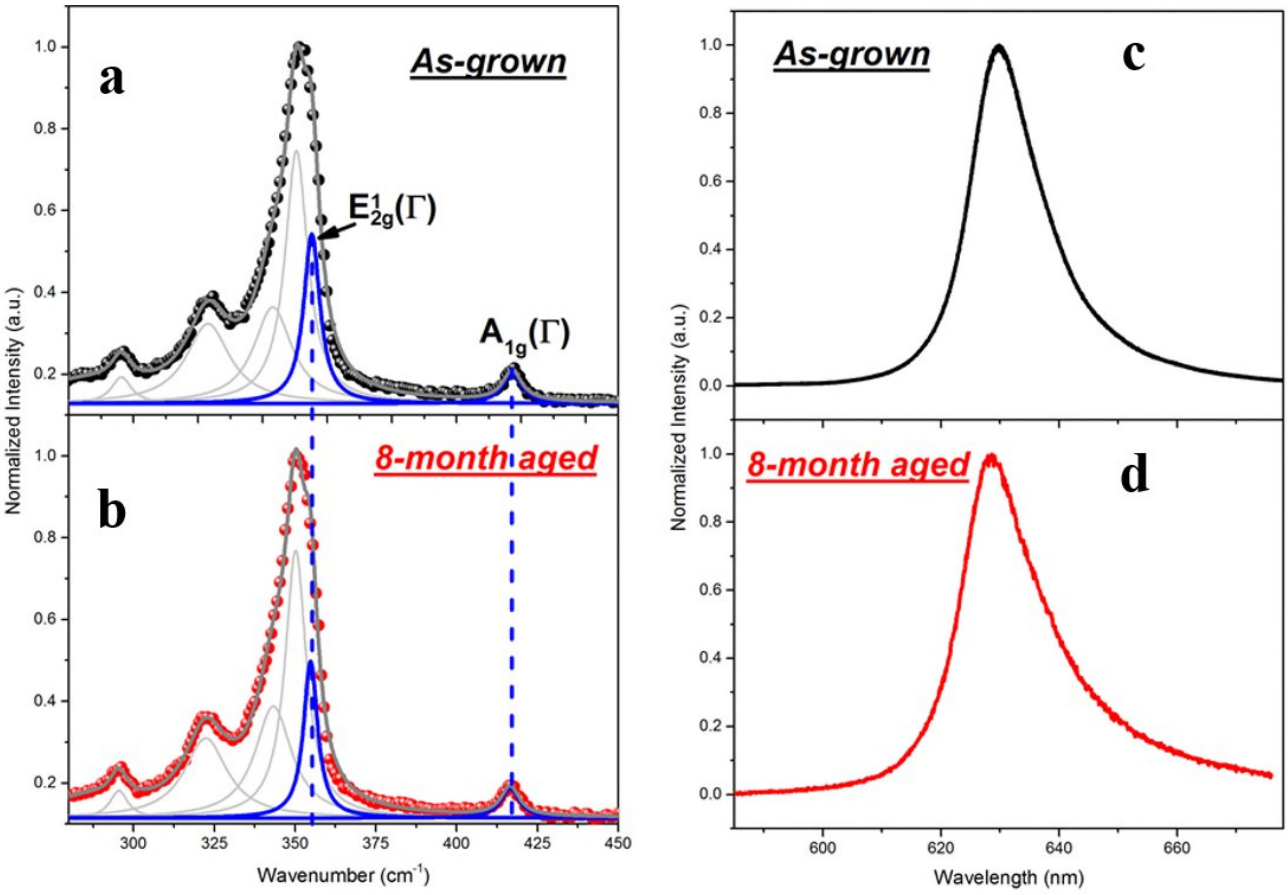

Figure 3. (a,b) Room temperature normalized Raman spectra of (a) as-grown and (b) 8-month aged monolayer WS_2. (c,d) Room temperature normalized PL of (c) as-grown and (d) 8-month aged WS_2. In (a) and (b), black and red spheres were experimental data. Light gray and blue curves were deconvolution results. Dark grey curves were the cumulative results.

Cryogenic PL spectroscopy can reveal more intrinsic properties of materials that cannot be seen at room temperature.[36,37] In figure 4(a),(c), we present the PL spectra from regions with similar optical contrast of both as-grown and 8-month aged sample taken at liquid nitrogen (LN) temperature. Similar to previous reports,[37] there were two main features in the spectra. The shoulder at high energy side is attributed to the combination of excitons (~610 nm) and trion emission (~615 nm). The broad band at the low energy side originated from localized states (LS) which are believed to be adsorbents related.[38]

However, there is still no observable distinction between as-grown and 8-month aged samples. Previous report showed that mid-gap states induced by defects can be passivated by oxygen or other adsorbents.[39] The dominant LS emission in the PL spectra indicates that most of the photo-generated excitons are bound to adsorbents, which may greatly reduce the diffusion length of excitons. Surface adsorbents which are from the initial exposure to air can completely cover the WS_2 sheets. Defects are likely to be sparsely distributed on the WS_2 crystal compared to surface adsorbents. Therefore, surface adsorbents have larger possibility to trap excitons, which may inhibit the formation of defects bound excitons. As a result, defects related features can be hardly observed.

It is well known that laser irradiation can enhance the desorption process of molecules physisorbed on surfaces.[40] In figure 4(b),(d), we presents the PL spectra of as-grown and 8-month aged monolayer WS_2 irradiated by focused laser beam with incident power density of ~40 kW/cm^2 for 30 seconds. LS emission in both samples were suppressed greatly, indicating that some of the impurities on WS_2 in this area have been removed after laser exposure. As a result, the emission from excitons and trions relative to the LS emission were enhanced in as-grown sample after laser treatment, shown in figure 4(b). In contrast, a new luminescent feature with emission energy between LS and trions emerged after the laser treatment of 8-month aged sample, presented in figure 4d. Here we denoted this new peak as peak U. This feature can be observed under excitation power density of as low as 0.1 W/cm^2 (See supporting information). We've repeated the measurement on more than 20 8-month aged crystals which all exhibited similar behavior. The peak positions ranged from 622 nm to 628 nm, similar to what has been reported in previous literature, where defects were created intentionally by exposing to water vapor.[31] For many applications, transferring WS_2 to other substrates is inevitable, where polymer scaffold is necessary. Considering that peak U can be hidden by adsorbents from air, polymer residual can also have the similar effect. Therefore, it is necessary to verify whether this method can be extended to transferred sample. As shown in figure 4(e),(f), similar phenomenon can also be observed on 8-month aged sample after being transferred from growth substrate to a new substrates. Figure 4(e)

shows the typical cryogenic PL spectrum of transferred monolayer WS_2 with three main features originating from excitons (591 nm), trions (602 nm),[41] and LS emission. Compared with non-transferred sample, the PL peak positions of excitons and trions of transferred crystal have a blue shift due to strain releasing while the LS redshifts. After laser treatment (~40 kW/cm^2, 10 seconds), luminescence of LS became much weaker while peak U emerged with similar emission energy to defects related PL peak reported in other literature.[41] Although the resemblance of peak positions with other literatures and distinct behaviour of as-grown and 8-month aged sample, it is still essential to exclude several other possible mechanisms before we can assign peak U to defects related emission. Noting that peak position of peak U in non-transferred sample resembles that of biexciton emission in monolayer WS_2,[37] we examined the power dependence of peak U in both non-transferred and transferred samples, plotted in figure 4(g),(h). Both exhibited linear power dependence, excluding that peak U was related to higher excitonic effects, in which a superlinear power dependence is expected.[36,37]

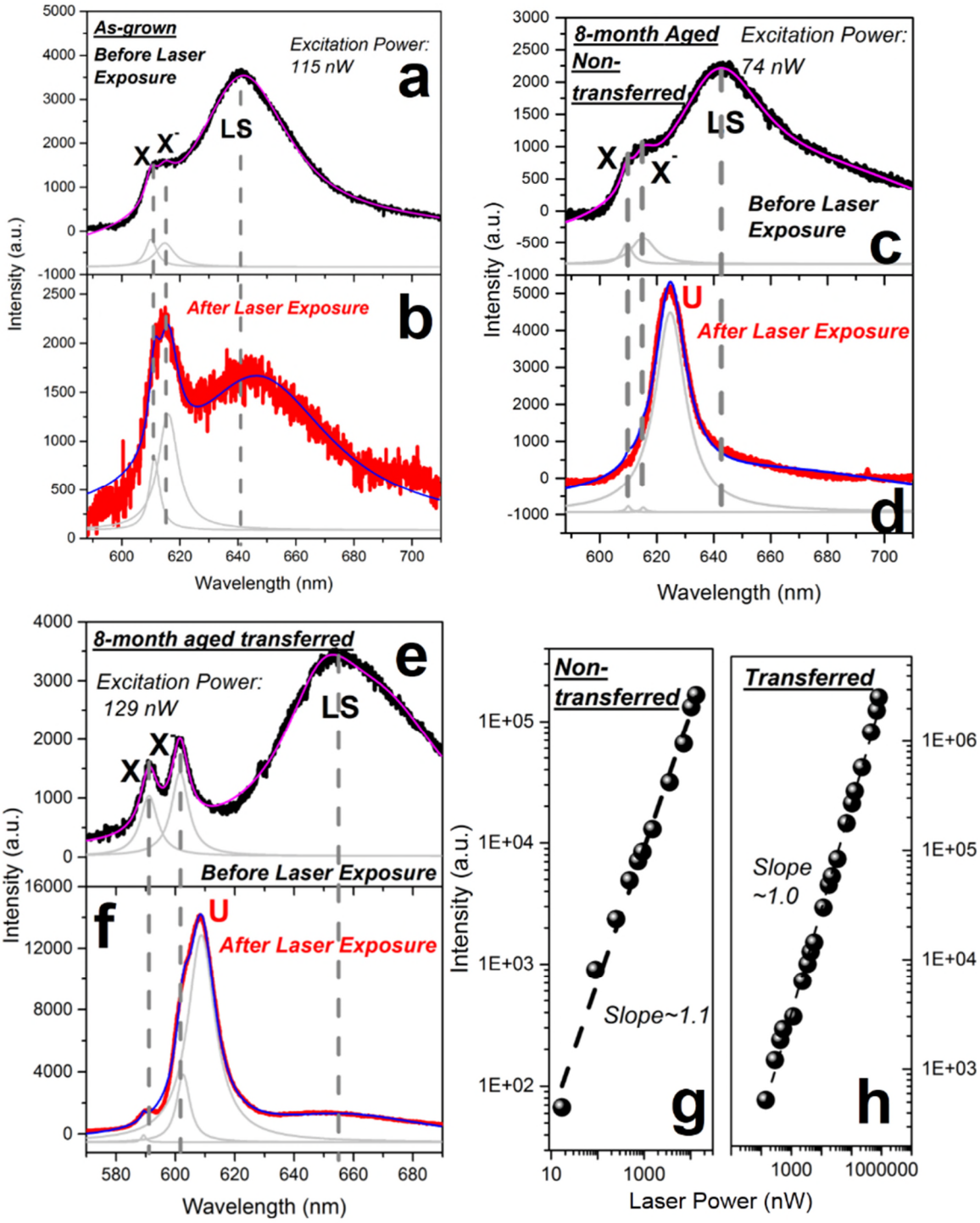

Figure 4. (a,b) PL spectra of as-grown (a) before and (b) after laser irradiation at 77 K. (c,d) PL spectra of 8-month aged sample (c) before and (d) after laser irradiation at 77 K. (e,f) PL spectra of 8-month aged transferred monolayer WS_2 at 77 K. (e) before and (f) after laser treatment. (g,h) Power dependence of peak U of (g) non-transferred and (h) transferred sample.

Exposure to lower laser power density of ~8 kW/cm^2 can also induce the PL transitions, but at a slower rate. In figure 5a, the PL evolution of 8-month aged non-transferred monolayer WS_2 varying with exposure time while keeping the exposure power density fixed at ~8 kW/cm^2. The black curve is the typical PL spectrum of aged monolayer WS_2 without laser treatment. After 1 sec laser irradiation, LS was suppressed yet still observable, accompanied by the emergence of peak U. We then performed the exposure treatment at the same point under a fixed laser power with increasing time. Obviously, LS emission was dimmer along with increasing peak U, depicted by the blue and pink curves in figure 5(a). No further obvious change occurred after 10 minutes exposure regardless of increasing exposure time or irradiation power. Similar behaviour can also be observed on transferred sample, shown in figure 5(b). The input energy from laser irradiation may lead to 2H-to-1T phase transition of WS_2, which can, as a consequence, alter its PL emission. However, 1T phase WS_2 crystals are metallic and therefore PL is completely suppressed.[42] Along with the evolutionary behavior of this phenomenon, we can rule out possibility that the change in PL was a result of laser induced phase transition.

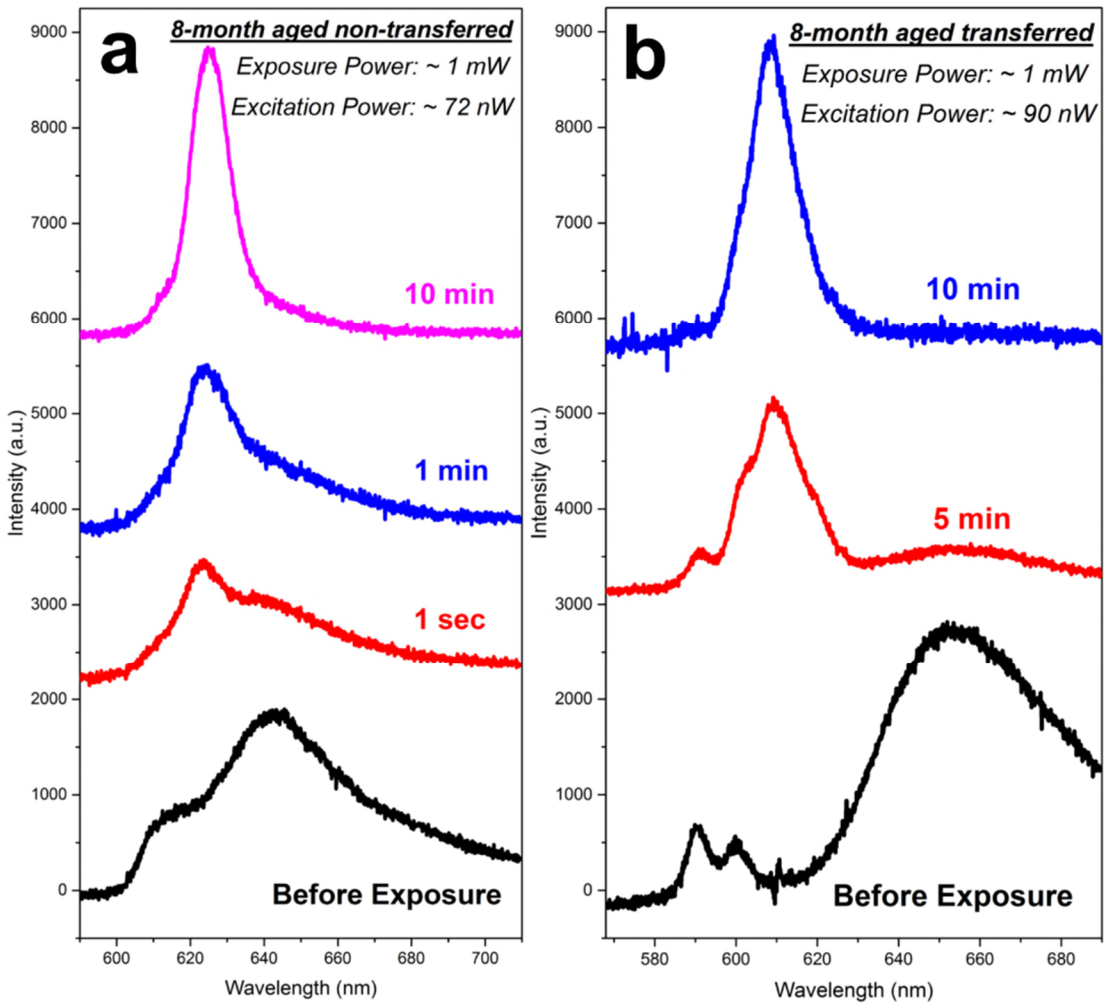

Figure 5. (a) PL shape evolution varying with laser exposure time of 8-month aged non-transferred monolayer WS_2 at 77 K. Black curve: before laser exposure. Red curve: 1 second exposure. Blue: 1 minute exposure. Pink: 10 minutes exposure. Exposure laser power density is fixed at ~ 8 kW/cm^2. (b) PL evolution of 8-month aged transferred sample at 77 K. Black curve: before laser exposure. Red curve: 5 min exposure. Blue curve: 10 minutes exposure.

This phenomenon was stable for at least 12 hours if kept in cryogenic environment, probably due to the fact that impurities were frozen at LN temperature and therefore few impurities can diffuse to the laser treated clean area from a surrounding "dirty" area. At room temperature, the mobilization of impurities can be activated and the laser treated area can be covered by impurities. As a result, peak U should disappear after a temperature cycle between 77 K and room temperature, in which WS_2 is first heated up to room temperature and then cooled back down to 77 K. Figure 6 shows results of both

non-transferred and transferred sample after laser treatment and then a thermal cycle, which present that peak U can be created or removed controllably by laser treatment and thermal cycling. In figure 6(a), peak U was created under ~8 kW/cm^2 laser exposure for 5 minutes. After that we gradually ramped the temperature to room temperature and then cool it down back to LN temperature. In figure 6(b), we presented the PL spectrum after the thermal cycle (blue curve) and the spectrum before laser exposure (orange dotted line) show that peak U disappears and PL spectrum changes back to its original shape with LS emission revived. Again, similar behavior can be realized on transferred WS_2 crystals, presented in figure 6(c,d). Based on the foregoing discussion, we believe that peak U be assigned as a degradation-related luminescent feature.

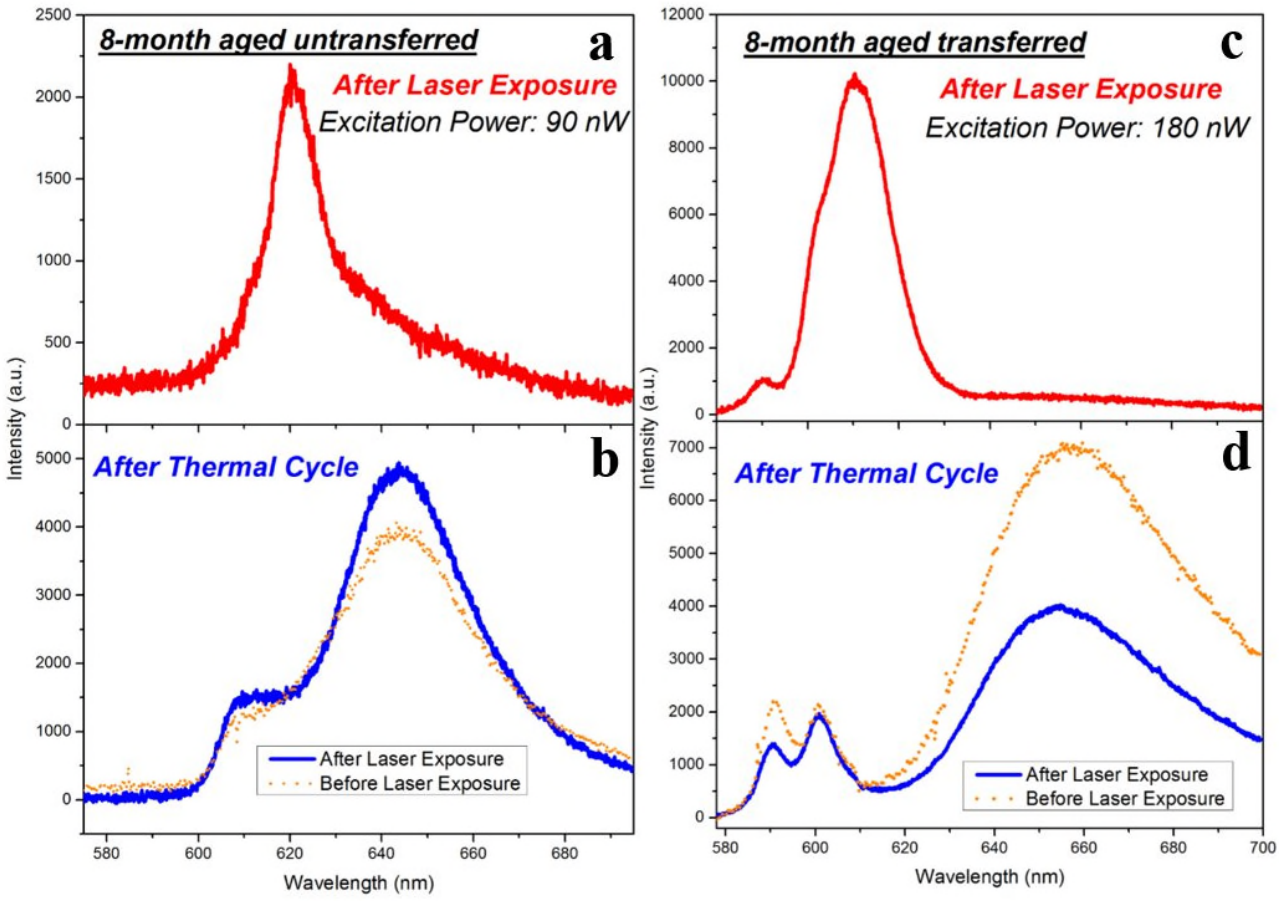

Figure 6. Thermal cycle effect on luminescent properties. (a) PL spectrum of aged non-transferred sample after laser exposure at 77 K. (b) PL spectrum of laser treated sample after thermal cycle at 77 K. Orange dotted line: PL spectrum at 77 K before laser exposure for comparison. (c) PL spectra at 77 K of laser treated transferred

sample before thermal cycle. (d) PL spectra after thermal cycle (blue curve) and before laser treatment (orange dotted line).

In figure 7 we employed this technique to monitor the degradation of monolayer WS_2 as a function of ageing time. In the first week, the PL spectrum of WS_2 after laser processing (~ 8 kW/cm^2, 10 minutes) looks very similar to that of as-grown sample. Further increasing the ageing time can lead to the emergence of peak U. Three weeks later, a shoulder (labelled by red dashed ellipse in figure 7b) appears at ~ 625 nm in the PL spectrum after laser processing. In the 5th week, peak U is well resolved, as shown in figure 7c. After 7-week ageing time, peak U dominates the whole spectrum after laser processing while at this stage, no visible optical contrast can be observed, indicating that our technique possesses high sensitivity towards degradation in WS_2, which may also have the potential to be extended to other TMD materials for quality characterization. In figure 7e, the weights of the PL integrated intensities of peak U extracted by peaks fitting over those of the whole PL spectra as a function of ageing time is presented, which clearly shows that peak U emission is gradually dominating the PL emission from WS_2 with increasing ageing time. (More spectra and curve fitting results can be found in supplementary information).

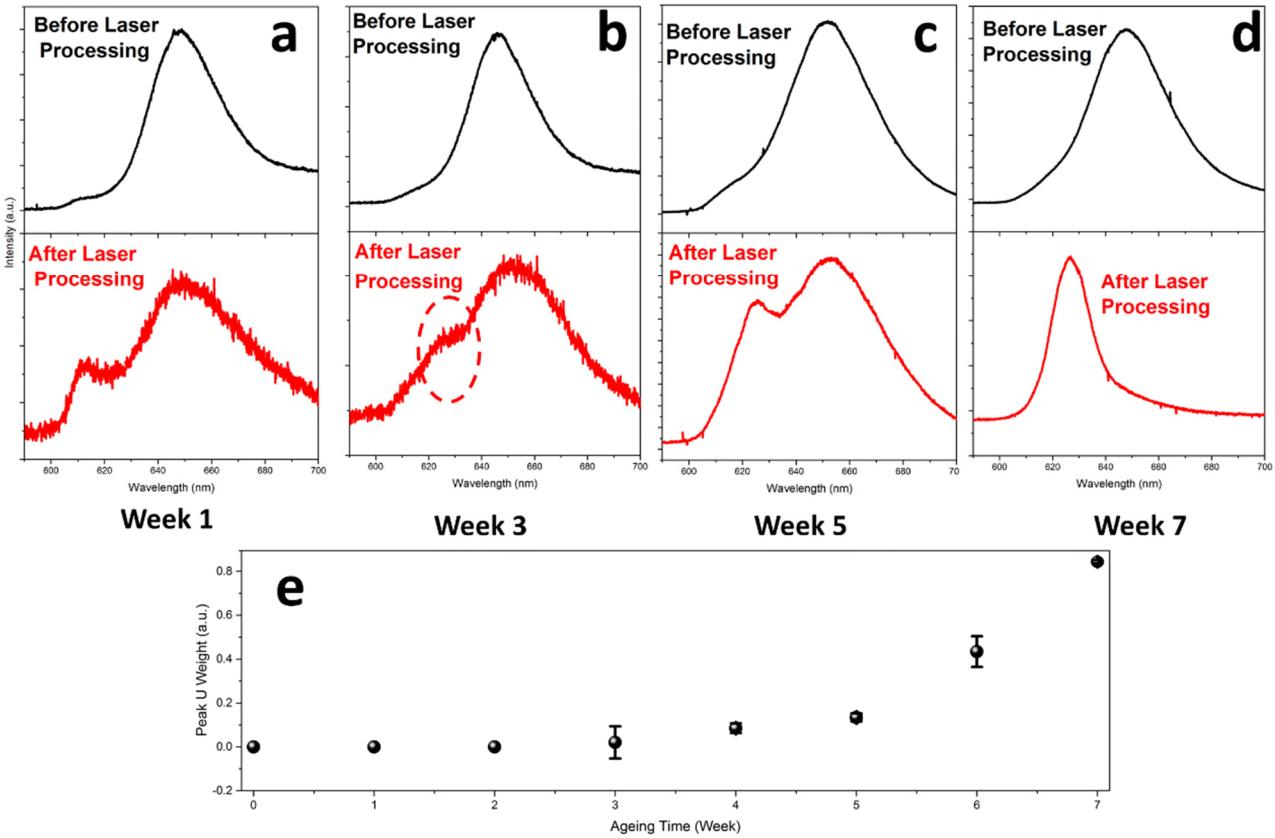

Figure 7. Typical PL spectra before and after laser processing of monolayer WS_2 aged in air for a) 1 week, b) 3 weeks, c) 5 weeks and d) 7 weeks. (e) Relative weight of Peak U (integrated intensity of U) with respect to the whole PL spectra as a function of the ageing time in air.

During the preparation of the manuscript, we noticed that Gao *et al.*[44] reported their observation of WS_2 and MoS_2. With the detailed analysis of XPS and Auger electron spectroscopy confirms that the degradation is a result of oxidation and organics adsorption. The time scale of degradation for both WS_2 and MoS_2 is about several months, which coincides with our observation. Such oxidation could lead to a reduction of source drain current by about 2 orders of magnitude.

Conclusion

This work shows how defects formed within monolayer WS_2 crystals left in air can be detected by low temperature PL, where laser induced cleaning can reveal unique emission states. Such a technique has the potential to be extended to other TMD materials, which could be useful for characterization of the

crystal quality. Carefully choosing the aging time along with the laser exposure may also lead to the WS_2 based single photon source, which has been realized in WSe_2.[45–48] Our results also demonstrate a controllable way to manipulate the luminescence wavelength between peak U and LS by utilizing the adsorbents on defective WS_2 *via* laser beam writing. This might have potential as a basic component for ultra-thin optical memory applications.[49]

Methods

Synthesis and Transfer of WS_2:

WS_2 monolayer crystals are prepared using our previously reported CVD method with sulphur and WO_3 as the precursor.[28] Sulphur and WO_3 are placed in a 1 inch quartz tube running through two furnace systems to provide two heating zones. Vaporized sulphur and WO_3 are carried by flowing argon gas to the reaction zone, where WO_3 undergoes sulphurization. High quality and large area WS_2 domains with atomic layer thickness are synthesized on Si wafers with 300 nm SiO_2 if proper parameters including temperature, Ar flow rate, sulphur introduction time are achieved.

During the transfer process, a thin layer of PMMA (495 K, A8, MicroChem) was spin coated onto the as-grown sample, followed by an etching process in which PMMA coated samples floated on 1 mol/L KOH (Sigma Aldrich) solution immersed water bath at 45°C for about 1 hr. The detached film was then transferred to target substrate. In this case, the target substrate was SiO_2/Si wafer.

PL and Raman Measurement:

The room temperature PL and Raman measurement in figure 1 and figure 2 are performed in a Jobin Yvon LabRam Aramis confocal-microscope based Raman spectroscopy using the 532 nm laser as excitation wavelength. PL spectra were acquired with power of about 20 μW while Raman spectra were acquired with excitation power of 2 mW.

In the cryogenic photoluminescence (PL) measurement, a 532 nm diode-pumped solid state laser (Thorlabs, DJ532-40) was used for excitation, with excitation power impinging onto sample ranging from ~100 nW to 10 mW. The laser was reflected off a dichroic beam splitter and focused to a spot size of ~2μm by 50x ultra-long working distance objective (Nikon, NA 0.45). WS_2 was placed in a flow microscopy cryostat (Janis, ST-500) with continuous liquid nitrogen flowing to keep the temperature constant at 77 K under vacuum of $\sim 1 \times 10^{-6}$ mbar. PL spectra were collected by a custom-built confocal microscope coupled to a spectrometer with an attached CCD (Princeton Instruments Acton SP-2300 spectrometer with Princeton Instruments, PIXIS 100 CCD).

Supporting Information

The Supporting Information is available free of charge on the ACS Publication website http://pubs.acs.org/. Raman spectrum of monolayer WS_2. Examples of peak U emergence in laser processed aged WS2 samples. PL spectrum after laser processing at low excitation power. Testing laser induced damage by Raman spectroscopy and optical microscopy. Power dependent PL colour maps. Morphology characterization of WS_2 before and after heating treatments. PL spectra as a function of time for aged WS_2 samples.

Acknowledgments

J.H.W. thanks the Royal Society for support. Z. H. thanks the China Scholarship Council and China Oxford Scholarship Fund for support.

References

(1) Mak, K. F.; Lee, C.; Hone, J.; Shan, J.; Heinz, T. F. Atomically Thin MoS_2: A New Direct-Gap Semiconductor. *Phys. Rev. Lett.* **2010**, *105*, 136805.

(2) Splendiani, A.; Sun, L.; Zhang, Y.; Li, T.; Kim, J.; Chim, C.-Y.; Galli, G.; Wang, F. Emerging Photoluminescence in Monolayer MoS_2. *Nano Lett.* **2010**, *10*, 1271–1275.

(3) Cao, T.; Wang, G.; Han, W.; Ye, H.; Zhu, C.; Shi, J.; Niu, Q.; Tan, P.; Wang, E.; Liu, B.; Feng, J. Valley-Selective Circular Dichroism of Monolayer Molybdenum Disulphide. *Nat. Commun.* **2012**, *3*, 887.

(4) Mak, K. F.; He, K.; Shan, J.; Heinz, T. F. Control of Valley Polarization in Monolayer MoS_2 by Optical Helicity. *Nat. Nanotechnol.* **2012**, *7*, 494–498.

(5) Xiao, D.; Liu, G. Bin; Feng, W.; Xu, X.; Yao, W. Coupled Spin and Valley Physics in Monolayers of MoS_2 and Other Group-VI Dichalcogenides. *Phys. Rev. Lett.* **2012**, *108*, 196802.

(6) Fang, H.; Battaglia, C.; Carraro, C.; Nemsak, S.; Ozdol, B.; Kang, J. S.; Bechtel, H. A; Desai, S. B.; Kronast, F.; Unal, A. A; Conti, G.; Conlon, C.; Palsson, G. K.; Martin, M. C.; Minor, A. M.; Fadley, C. S.; Yablonovitch, E.; Maboudian, R.; Javey, A. Strong Interlayer Coupling in van Der Waals Heterostructures Built from Single-Layer Chalcogenides. *Proc. Natl. Acad. Sci. U. S. A.* **2014**, *111*, 6198–6202.

(7) Ramasubramaniam, A. Large Excitonic Effects in Monolayers of Molybdenum and Tungsten Dichalcogenides. *Phys. Rev. B* **2012**, *86*, 115409.

(8) Gutiérrez, H. R.; Perea-López, N.; Elías, A. L.; Berkdemir, A.; Wang, B.; Lv, R.; López-Urías, F.; Crespi, V. H.; Terrones, H.; Terrones, M. Extraordinary Room-Temperature Photoluminescence in Triangular WS_2 Monolayers. *Nano Lett.* **2013**, *13*, 3447–3454.

(9) Peimyoo, N.; Shang, J.; Cong, C.; Shen, X.; Wu, X.; Yeow, E. K. L.; Yu, T. Nonblinking, Intense Two-Dimensional Light Emitter: Monolayer WS_2 Triangles. *ACS Nano* **2013**, *7*, 10985–10994.

(10) Mai, C.; Barrette, A.; Yu, Y.; Semenov, Y. G.; Kim, K. W.; Cao, L.; Gundogdu, K. Many-Body Effects in Valleytronics: Direct Measurement of Valley Lifetimes in Single-Layer MoS_2. *Nano Lett.* **2014**, *14*, 202–206.

(11) Lopez-Sanchez, O.; Lembke, D.; Kayci, M.; Radenovic, A.; Kis, A. Ultrasensitive Photodetectors Based on Monolayer MoS_2. *Nat. Nanotechnol.* **2013**, *8*, 497–501.

(12) Perea-López, N.; Elías, A. L.; Berkdemir, A.; Castro-Beltran, A.; Gutiérrez, H. R.; Feng, S.; Lv, R.; Hayashi, T.; López-Urías, F.; Ghosh, S.; Muchharla, B.; Talapatra, S.; Terrones, H.; Terrones, M. Photosensor Device Based on Few-Layered WS_2 Films. *Adv. Funct. Mater.* **2013**, *23*, 5511–5517.

(13) Perea-López, N.; Lin, Z.; Pradhan, N. R.; Iñiguez-Rábago, A.; Laura Elías, A.; McCreary, A.; Lou, J.; Ajayan, P. M.; Terrones, H.; Balicas, L.; Terrones, M. CVD-Grown Monolayered MoS_2 as an Effective Photosensor Operating at Low-Voltage. *2D Mater.* **2014**, *1*, 011004.

(14) Pospischil, A.; Furchi, M. M.; Mueller, T. Solar-Energy Conversion and Light Emission in an Atomic Monolayer P-N Diode. *Nat. Nanotechnol.* **2014**, *9*, 257–261.

(15) Wi, S.; Kim, H.; Chen, M.; Nam, H.; Guo, L. J.; Meyhofer, E.; Liang, X. Enhancement of Photovoltaic Response in Multilayer MoS_2 Induced by Plasma Doping. *ACS Nano* **2014**, *8*, 5270–5281.

(16) Lopez-Sanchez, O.; Alarcon Llado, E.; Koman, V.; Fontcuberta i Morral, A.; Radenovic, A.; Kis, A. Light Generation and Harvesting in a van Der Waals Heterostructure. *ACS Nano* **2014**, *8*, 3042–3048.

(17) Bernardi, M.; Palummo, M.; Grossman, J. C. Extraordinary Sunlight Absorption and One Nanometer Thick Photovoltaics Using Two-Dimensional Monolayer Materials. *Nano Lett.* **2013**, *13*, 3664–3670.

(18) Baugher, B. W. H.; Churchill, H. O. H.; Yang, Y.; Jarillo-Herrero, P. Optoelectronic Devices Based on Electrically Tunable P-N Diodes in a Monolayer Dichalcogenide. *Nat. Nanotechnol.* **2014**, *9*, 262–267.

(19) Ross, J. S.; Klement, P.; Jones, A. M.; Ghimire, N. J.; Yan, J.; Mandrus, D. G.; Taniguchi, T.; Watanabe, K.; Kitamura, K.; Yao, W.; Cobden, D. H.; Xu, X. Electrically Tunable Excitonic Light-Emitting Diodes Based on Monolayer WSe_2 P-N Junctions. *Nat. Nanotechnol.* **2014**, *9*, 268–272.

(20) Kim, S.; Zhou, S.; Hu, Y.; Acik, M.; Chabal, Y. J.; Berger, C.; de Heer, W.; Bongiorno, A.; Riedo, E. Room-Temperature Metastability of Multilayer Graphene Oxide Films. *Nat. Mater.* **2012**, *11*, 544–549.

(21) Wood, J. D.; Wells, S. a; Jariwala, D.; Chen, K.; Cho, E.; Sangwan, V. K.; Liu, X.; Lauhon, L. J.; Marks, T. J.; Hersam, M. C. Effective Passivation of Exfoliated Black Phosphorus Transistors Against Ambient Degradation. *Nano Lett.* **2014**, *14*, 6964–6970.

(22) Doganov, R. a.; O'Farrell, E. C. T.; Koenig, S. P.; Yeo, Y.; Ziletti, A.; Carvalho, A.; Campbell, D. K.; Coker, D. F.; Watanabe, K.; Taniguchi, T.; Neto, A. H. C.; Özyilmaz, B. Transport Properties of Pristine Few-Layer Black Phosphorus by van Der Waals Passivation in an Inert Atmosphere. *Nat. Commun.* **2015**, *6*, 6647.

(23) Park, K.; Beule, C. De; Partoens, B. The Ageing Effect in Topological Insulators: Evolution of the Surface Electronic Structure of Bi_2Se_3 upon K Adsorption. *New J. Phys.* **2013**, *15*, 113031.

(24) Rumyantsev, S.; Liu, G.; Stillman, W.; Shur, M.; Balandin, A. A. Electrical and Noise Characteristics of Graphene Field-Effect Transistors: Ambient Effects, Noise Sources and Physical Mechanisms. *J. Phys. Condens. Matter* **2010**, *22*, 395302.

(25) Novoselov, K. S.; Fal'ko, V. I.; Colombo, L.; Gellert, P. R.; Schwab, M. G.; Kim, K. A Roadmap for Graphene. *Nature* **2012**, *490*, 192–200.

(26) Zhang, Y.; Zhang, Y.; Ji, Q.; Ju, J.; Yuan, H.; Shi, J.; Gao, T. Controlled Growth of High-Quality Monolayer WS_2 Layers on Sapphire and Imaging Its Grain Boundary. *ACS Nano* **2013**, *7*, 8963–8971.

(27) Rong, Y.; He, K.; Robertson, A. W.; Bhaskaran, H.; Warner, J. H. Controlled Preferential Oxidation of Grain Boundaries in Monolayer Tungsten Disulfide for Direct Optical Imaging. *ACS Nano* **2015**, *9*, 3695–3703.

(28) Rong, Y.; Fan, Y.; Leen Koh, A.; Robertson, A. W.; He, K.; Wang, S.; Tan, H.; Sinclair, R.; Warner, J. H. Controlling Sulphur Precursor Addition for Large Single Crystal Domains of WS_2. *Nanoscale* **2014**, *6*, 12096–12103.

(29) Liang, T.; Sawyer, W. G.; Perry, S. S.; Sinnott, S. B.; Phillpot, S. R. Energetics of Oxidation in MoS_2 Nanoparticles by Density Functional Theory. *J. Phys. Chem. C* **2011**, *115*, 10606–10616.

(30) Santosh, K. C.; Longo, R. C.; Wallace, R. M.; Cho, K. Surface Oxidation Energetics and Kinetics on MoS_2 Monolayer. *J. Appl. Phys.* **2015**, *117*, 135301.

(31) Kato, T.; Kaneko, T. Optical Detection of a Highly Localized Impurity State in Monolayer Tungsten Disulfide. *ACS Nano* **2014**, *8*, 12777–12785.

(32) Ferrari, A. C.; Meyer, J. C.; Scardaci, V.; Casiraghi, C.; Lazzeri, M.; Mauri, F.; Piscanec, S.; Jiang, D.; Novoselov, K. S.; Roth, S.; Geim, A. K. Raman Spectrum of Graphene and Graphene Layers. *Phys. Rev. Lett.* **2006**, *97*, 187401.

(33) Berkdemir, A.; Gutiérrez, H. R.; Botello-Méndez, A. R.; Perea-López, N.; Elías, A. L.; Chia, C.-I.; Wang, B.; Crespi, V. H.; López-Urías, F.; Charlier, J.-C.; Terrones, H.; Terrones, M. Identification of Individual and Few Layers of WS_2 Using Raman Spectroscopy. *Sci. Rep.* **2013**, *3*, 1755.

(34) Tongay, S.; Suh, J.; Ataca, C.; Fan, W.; Luce, A.; Kang, J. S.; Liu, J.; Ko, C.; Raghunathanan, R.; Zhou, J.; Ogletree, F.; Li, J.; Grossman, J. C.; Wu, J. Defects Activated Photoluminescence in Two-Dimensional Semiconductors: Interplay between Bound, Charged, and Free Excitons. *Sci. Rep.* **2013**, *3*, 2657.

(35) Chow, P. K.; Jacobs-Gedrim, R. B.; Gao, J.; Lu, T.-M.; Yu, B.; Terrones, H.; Koratkar, N. Defect-Induced Photoluminescence in Monolayer Semiconducting Transition Metal Dichalcogenides. *ACS Nano* **2015**, *9*, 1520–1527.

(36) You, Y.; Zhang, X.-X.; Berkelbach, T. C.; Hybertsen, M. S.; Reichman, D. R.; Heinz, T. F. Observation of Biexcitons in Monolayer WSe_2. *Nat. Phys.* **2015**, *11*, 477–481.

(37) Shang, J.; Shen, X.; Cong, C.; Peimyoo, N.; Cao, B.; Eginligil, M. Observation of Excitonic Fine Structure in a 2D Transition-Metal Dichalcogenide Semiconductor. *ACS Nano* **2015**, *9*, 647–655.

(38) Plechinger, G.; Schrettenbrunner, F. X.; Eroms, J.; Weiss, D.; Schüller, C.; Korn, T. Low-Temperature Photoluminescence of Oxide-Covered Single-Layer MoS_2. *Phys. Status Solidi - Rapid Res. Lett.* **2012**, *6*, 126–128.

(39) Liu, Y.; Stradins, P.; Wei, S. H. Air Passivation of Chalcogen Vacancies in Two-Dimensional Semiconductors. *Angew. Chemie - Int. Ed.* **2016**, *55*, 965–968.

(40) Shiang, K.-D. Quantum-Mechanical Study of Laser Induced Desorption of Physisorbed Molecules on Dielectric Surfaces. *Surf. Sci.* **1993**, *292*, 145–148.

(41) Plechinger, G.; Nagler, P.; Kraus, J.; Paradiso, N.; Strunk, C.; Schüller, C.; Korn, T. Identification of Excitons, Trions and Biexcitons in Single-Layer WS_2. *Phys. status solidi - Rapid Res. Lett.* **2015**, *9*, 457–461.

(42) Voiry, D.; Goswami, A.; Kappera, R.; Silva, C. de C. C. e; Kaplan, D.; Fujita, T.; Chen, M.; Asefa, T.; Chhowalla, M.; Carvalho Castro e Silva, C. De; Kaplan, D.; Fujita, T.; Chen, M.; Asefa, T.; Chhowalla, M. Covalent Functionalization of Monolayered Transition Metal Dichalcogenides by Phase Engineering. *Nat. Chem.* **2014**, *7*, 45–49.

(43) Wang, S.; Wang, X.; Warner, J. H. All Chemical Vapor Deposition Growth of MoS_2 : H-BN Vertical van Der Waals Heterostructures. *ACS Nano* **2015**, *9*, 5246–5254.

(44) Gao, J.; Li, B.; Tan, J.; Chow, P.; Lu, T.-M.; Koratkar, N. Aging of Transition Metal Dichalcogenide Monolayers. *ACS Nano* **2016**, *10*, 2628–2635.

(45) Srivastava, A.; Sidler, M.; Allain, A. V.; Lembke, D. S.; Kis, A.; Imamoğlu, A. Optically Active Quantum Dots in Monolayer WSe_2. *Nat. Nanotechnol.* **2015**, *10*, 491–496.

(46) Chakraborty, C.; Kinnischtzke, L.; Goodfellow, K. M.; Beams, R.; Vamivakas, A. N. Voltage-Controlled Quantum Light from an Atomically Thin Semiconductor. *Nat. Nanotechnol.* **2015**, *10*, 507–511.

(47) Koperski, M.; Nogajewski, K.; Arora, A.; Cherkez, V.; Mallet, P.; Veuillen, J.-Y.; Marcus, J.; Kossacki, P.; Potemski, M. Single Photon Emitters in Exfoliated WSe_2 Structures. *Nat. Nanotechnol.* **2015**, *10*, 503–506.

(48) He, Y.-M.; Clark, G.; Schaibley, J. R.; He, Y.; Chen, M.-C.; Wei, Y.-J.; Ding, X.; Zhang, Q.; Yao, W.; Xu, X.; Lu, C.-Y.; Pan, J.-W. Single Quantum Emitters in Monolayer Semiconductors. *Nat. Nanotechnol.* **2015**, *10*, 497–502.

(49) Gu, M.; Li, X.; Cao, Y. Optical Storage Arrays: A Perspective for Future Big Data Storage. *Light Sci. Appl.* **2014**, *3*, e177.

TOC graphic

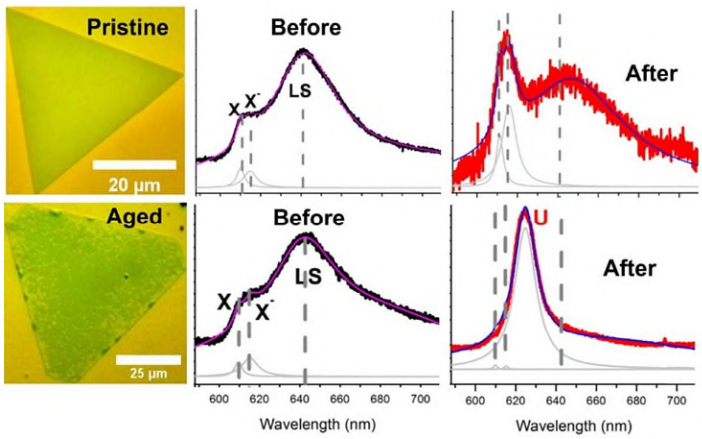
Pristine
20 μm
Before
X
X-
LS
After
Aged
25 μm
Before
X
X-
LS
U
After
600
620
640
660
680
700
Wavelength (nm)
600
620
640
660
680
700
Wavelength (nm)